Viscous Water Meniscus under Nanoconfinement

R. C. Major,[1] J. E. Houston,[2] M. J. McGrath,[1] J. I. Siepmann,[1] and X.-Y. Zhu[1]
[1]*Department of Chemistry, University of Minnesota, Minneapolis, Minnesota 55455, USA*
[2]*Sandia National Laboratory, Albuquerque, New Mexico 87185, USA*
(Received 5 November 2005; published 5 May 2006)

A dramatic transition in the mechanical properties of water is observed at the nanometer scale. For a water meniscus formed between two hydrophilic surfaces in the attractive region, with ≤ 1 nm interfacial separation, the measured viscosity is 7 orders of magnitude greater than that of bulk water at room temperature. Grand canonical Monte Carlo simulations reveal enhancement in the tetrahedral structure and in the number of hydrogen bonds to the surfaces as a source for the high viscosity; this results from a cooperative effect of hydrogen bonding of water molecules to both hydrophilic surfaces.

DOI: 10.1103/PhysRevLett.96.177803 PACS numbers: 62.10.+s, 61.46.−w, 66.20.+d

Water molecules confined between interfaces with nanoscopic separation are of critical importance in many fields. Examples include, among others, hydration forces in biology and colloid science [1], swelling of layered clays [2], and capillary forces in scanning probe microscopy and nanolithography [3,4]. Despite the broad interest, little is known about the properties of water confined between two surfaces with nanoscopic separation, where macroscopic theories for capillary condensation are expected to break down [3]. ''Structured'' water at interfaces has long been thought to explain a wide range of physical, chemical, biological, and geological processes. Because of experimental difficulties in probing a nanoscopic solid-water-solid interface, most studies on interfacial water have dealt with solid-water interfaces using, e.g., vibrational spectroscopies [5–7], atomic force microscopy (AFM) [8], and x-ray diffraction [9]. In principle, AFM may be used to probe the nanoscopic water meniscus, but quantitative measurements are difficult because sensor instability results in the well-known ''jump-to-contact'' in the attractive region. Similar difficulties are encountered in experiments based on the surface force apparatus (SFA) [10], which accordingly has been used to probe confined molecules only in the repulsive region. SFA studies by Granick and co-workers showed very high effective viscosity of liquid films, including water, confined between two mica surfaces [11,12]. This is in agreement with a shear force microscopy study which showed the rapid rise in viscosity of confined water as interfacial separation decreases below 1 nm [13]. By contrast, Klein and co-workers reported the fluidic nature of water confined between mica surfaces at <3.5 nm interfacial separation, with bulk-water–like viscosity [14]. An earlier measurement showed bulklike viscosity of water confined between two mica surfaces with interfacial separation ≥ 2 nm [15]. An AFM study also suggested the lubricative effects of adsorbed water [16].

Here we probe the mechanical properties of the water meniscus in the attractive region between two chemically distinct surfaces using interfacial force microscopy (IFM) (schematic illustration in Fig. 1, detailed in Ref. [17]) whose self-balancing, force-feedback sensor eliminates the mechanical instability problem and allows quantitative measurements of normal and lateral (shear) forces throughout the entire range of interfacial separation. We use a single-crystal Au(111) and an electrochemically etched parabolic Au tip ($R = 500$ nm). Each Au surface is made hydrophilic or hydrophobic by the chemisorption of a COOH or CH_3 terminated alkanethiol self-assembled monolayer (SAM). After standard cleaning, the Au sample is immersed in ethanol solutions of mercaptoundecanoic acid [HS-$(CH_2)_{10}$-COOH, 0.5 mM, 5% acetic acid] or hexadecanethiol [HS-$(CH_2)_{15}$-CH_3, 0.5 mM] to form

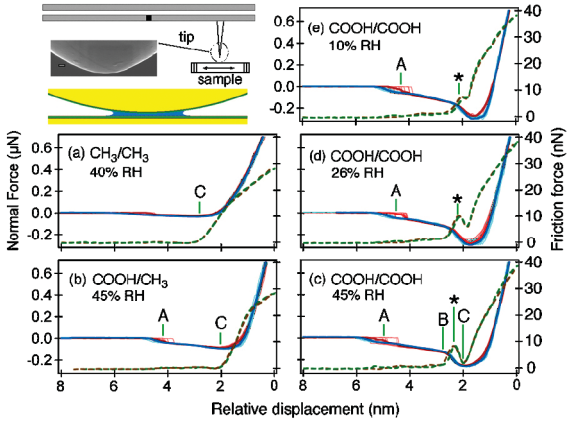

FIG. 1 (color). Schematic: experimental system. The scanning electron microscope image shows the parabolic Au tip with radius of curvature of 500 nm. (a)–(e) Normal force (F_N, solid curves and left axis) and friction force (F_μ, dashed curves and right axis) profiles as a function of relative displacement between the tip and the sample at the indicated RH values for the following interface combinations: (a) CH_3 tip on CH_3 surface; (b) COOH tip on CH_3 surface; and (c)–(e) COOH tip on COOH surface. In each of the above panels, the thin pink and blue curves are individual F_N profiles during approach and retract, respectively; the thick red (approach) and blue (retract) curves are averaged data. Only averaged data are shown for F_μ profiles (dashed brown curves for approach and dashed green curves for retract). *A*, *B*, and*C* represent positions for water nucleation, capillary condensation, and film contact, respectively.

 © 2006 The American Physical Society

each SAM. In the case of -COOH terminated SAM, it is necessary to remove weakly adsorbed bilayers [18] by sonicating in 5% acetic acid/ethanol, rinsing in a 1 mM ethanolic solution of $Cu(NO_3)_2$ which displaces weakly adsorbed molecules [19], reprotonating the surface in 5% acetic acid/ethanol, and finally drying with N_2. The water contact angle on the -COOH terminated surface is $\leq 9°$ while that on the $-CH_3$ surface is $\sim 115°$. We measure the normal force (F_N) and friction force (F_μ) as a function of relative interfacial separation at 20 °C and 1 atm with controlled relative humidity (RH) $\leq 45\%$. Friction is measured by oscillating the tip laterally at 100 Hz and ~ 1 nm amplitude, and recording the resulting force signal synchronously. We have used larger oscillating amplitudes (up to 20 nm) and found the friction force to scale linearly with shear velocity.

Figure 1 shows normal- and friction-force profiles for (a) $-CH_3$ tip on $-CH_3$ surface, (b) -COOH tip on $-CH_3$ surface, and (c)–(e) -COOH tip on -COOH surface. Note that there are 12 independent measurements as well as the averaged data for each force profile. The excellent agreement from measurement to measurement shows that the experiment is highly reproducible. The zero point of relative displacement (RD) refers to the F_N value (1 μN) at which the tip begins its retraction. Also shown are the averaged friction data indicated by the heavy dashed lines.

When both surfaces are hydrophobic [panel (a)], the force profiles are virtually independent of RH (data not shown). There is a small attraction well before contact indicated by point C. After contact between the two films (C, at RD ~ 2.5 nm) the normal force begins its rise to the repulsive region and the friction force increases rapidly above zero. The repulsive region of the F_N profile can be analyzed within the Johnson-Kendall-Roberts (JKR) model [10] which describes deformable interfaces in the presence of an attractive potential. The JKR fit gives a composite modulus of 13 GPa. For comparison, fits to the $COOH/CH_3$ and COOH/COOH combinations give composite moduli of 29 and 33 GPa, respectively. The composite modulus increases in the order $CH_3/CH_3 < COOH/CH_3 <$ COOH/COOH, owing to different total molecular lengths of the SAM combinations [17]. The differences in the composite modulus are responsible for the different relative RD scales for the three panels.

Compared to CH_3/CH_3, the maximum attractive force for $COOH/CH_3$ increases about threefold [panel (b)]. The higher adhesion is due to the addition of a dipole—induced dipole component to the van der Waals (vdW) interaction due to the polar nature of the COOH surface (~ 2 D per COOH group), as well as capillary condensation of water on the COOH surface. The later serves to decrease the effective distance for the vdW interaction between the two surfaces. As the two surfaces approach, there is an attractive jump in F_N around point A (RD $\sim$ 4.2 nm). The scatter in this point is consistent with nucleation and capillary condensation; this is supported by simulation below. As the tip continues its approach, F_N begins a slow decrease up to approximately point C (RD ~ 2.0 nm), where F_N enters the repulsive region and F_μ rises rapidly. This point, again, corresponds to contact between the two films.

When both surfaces are hydrophilic [panel (c)], the magnitudes of the initial jump in F_N and the attractive force in the slow growth region (from point A to point B) are higher than those seen for the $COOH/CH_3$ combination. This is consistent with the nucleation and growth of water meniscus at the hydrophilic interface. A quantitative understanding of the jump in and the slow growth of attractive normal force requires realistic simulation at a scale not possible with current theoretical methods [3]. Here we focus on the most provocative aspect of experimental observation for confinement within ~ 1 nm of interfacial separation. The unique aspect of the COOH/COOH data is the rapid increase in attractive force beginning near point B (to a maximum value an order of magnitude larger than that in CH_3/CH_3). At virtually the same distance, the friction force begins a rapid rise. This is very different from the CH_3/CH_3 and $COOH/CH_3$ combinations, where the friction force only rises sharply at film contact (point C). This behavior strongly suggests capillary condensation to form a water meniscus, which is responsible for both F_N and F_μ. As expected for capillary condensation and water-meniscus formation, the F_N and F_μ profiles for the COOH/COOH interface depend on RH [panels (c)–(e) in Fig. 1]. At RH = 10%, presence of the peak in F_μ profile shows up as a shoulder (*), which grows as RH is increased to 45%. Note that F_N continues to rise until film/film contact (point C) whereas F_μ peaks (*) and then decreases to near baseline at point C, before rising again after film contact. This is because the meniscus is squeezed or swept away from the nanogap as the interfacial separation decreases beyond a critical point (*).

The cross sectional area (A_m) of the water meniscus can be obtained from the peak attractive normal force and the Kelvin radius (r_K) of the meniscus given by [10]

$$r_K = \frac{\gamma_{H_2O} V_M}{RT \ln(p/p_s)}, \quad (1)$$

where γ_{H_2O}, V_M, R, T, and p/p_s are the surface tension, the molar volume of the water meniscus, the gas constant, the absolute temperature, and the relative humidity, respectively. The Laplace pressure of the water meniscus is $P_L = \gamma_{H_2O}/r_K$ and the capillary force is $F_C = A_m P_L$. When the attractive normal force reaches a minimum, the maximum size of the meniscus is $A_m = 1000$, 1600, and 2400 nm^2 for RH = 10%, 26%, and 45%, respectively. The growth of the meniscus with RH is also shown by the outward shift of the point of meniscus nucleation (A) or capillary condensation (B) with increasing RH (right panels in Fig. 1).

The viscosity of the water meniscus must be significantly larger than that of bulk water since a submerged tip in water shows negligible friction force under the same

conditions. Given the peak friction-force value of $F_\mu{}^* = 8.6$ nN at 45% RH, and an experimental shear velocity of $c = 180$ nm/s, we can estimate the effective viscosity (η_{eff}) of the meniscus at the peak of $F_\mu{}^*$ using the model of Feibelman for a sphere on plate geometry [20]:

$$\eta_{\text{eff}} = \frac{-F_\mu{}^*}{-2\pi c R \ln(d^*/2w)} \approx 30 \text{ kPa} \cdot \text{s}, \qquad (2)$$

where $2w$ is the total thickness the viscous water films on the two surfaces and is taken to be the total width ($\sim$1 nm) of the F_μ peak in Fig. 1(c); R is tip radius; d^*($\sim$0.6 nm) is the interfacial distance at which the friction-force peaks. The estimated viscosity of the water meniscus is more than 7 orders of magnitude higher than the viscosity of bulk water ($\eta_{\text{bulk}} = 8.6 \times 10^{-4}$ Pa $\cdot$ s at room temperature). The value of η_{eff} for the water meniscus is similar to that reported for a quasiliquid layer on the ice surface [21] or to that estimated for a hydration layer on an oligo(ethylene glycol) surface [22]. The distance range for the viscous water layer is in agreement with a recent spectroscopic study which showed that structured water grew up to three layers thick on the silica surface [7].

We have carried out IFM measurements for a hydrophilic oxide terminated W tip and a hydrophilic oxide terminated Si(111) surface in the ambient and observed a viscous water meniscus with similar viscosity. The same viscosity is also observed when both the tip and the surface are immersed in water. The viscous water film disappears when the Si(111) surface is made more hydrophobic by H or CH_3 termination. Note that IFM measurements reported here required exceptional care in ensuring surface cleanliness and used only freshly prepared samples. Force profiles become irreproducible when the surfaces have been exposed to the ambient for more than $\sim$2 h.

Grand canonical Monte Carlo (MC) simulations provide microscopic-level information on the water meniscus confined in nanoscopic gaps. The methodology employed closely follows an earlier simulation study of the mechanical relaxation of SAMs [23]. The initial configuration for each run consisted of two layers of 56 SAM molecules, Au-S-$(CH_2)_{15}$(-COOH or -CH_3), placed in an orthorhombic simulation cell that is periodically replicated only in the substrate plane. The 7×8 array of molecules in a given layer is too small to show different tilt domains [24]; thus four independent simulations were run for each system to sample different tilt orientations of the opposing layers. After a lengthy initial equilibration, the approach/retract cycle was modeled by displacing the distance between the two substrates by an amount of 5×10^{-5} nm after every MC cycle (where one cycle consists of N trial moves with N being the instantaneous total number of SAM and water molecules). The simulation model was adopted from previous SAM simulations [23,24] with the TraPPE and TIP4P force fields used for chain segments and water, respectively [25,26]. Phase space was sampled at $T = 300$ K and RH = 10% through translations and rotations of entire molecules and coupled-decoupled configurational-bias MC moves [25] for the SAM's conformational degrees of freedom and for water insertions and deletions.

Figure 2 shows snapshots taken from COOH/COOH and COOH/CH_3 simulations during approach for three interfacial separations (D). For COOH/COOH at $D >$ 1 nm, the simulation shows mostly surface water molecules. At $D \leq 1$ nm, hydrogen-bonded water bridges connecting the two COOH surfaces start to appear. Further decrease in D leads to a rapid rise in the number of interfacial water molecules; this is capillary condensation. A snapshot at $D = 0.7$ nm clearly shows that the meniscus corresponds to an extensively hydrogen-bonded network connecting the two surfaces. When D decreases below 0.5 nm, the water molecules are squeezed out. For the COOH/CH_3 combination, the snapshots in Fig. 2 show fewer water molecules, but the formation of water clusters extending into the gap is still observed for 0.4 nm $< D <$ 1 nm.

The number of H_2O (N_A) within the simulation cell as a function of D is plotted in Fig. 3. For the COOH/COOH combination, the water population peaks at $D = 0.6$ or 1.0 nm (approach or retract). This distance is in excellent agreement with the experimental positions of peak friction force. The simulation yields an onset of capillary condensation at an interfacial separation of $\sim$1.0 nm, while the experimentally observed jump in occurs at $\sim$2.3 nm for RH = 10% [point A in Fig. 1(e)]. This level of discrepancy is not unexpected, given the much smaller size of the simulation cell. For the COOH/CH_3 combination, a smaller peak in water population is seen during approach; the peak is less obvious in retraction. The slow rise in water population as interfacial separation decreases from $\sim$3 nm to 0.6–0.9 nm is consistent with the shallow attractive well seen in the experimental F_N profile. Note that the simulations show significantly more hysteresis than experiment.

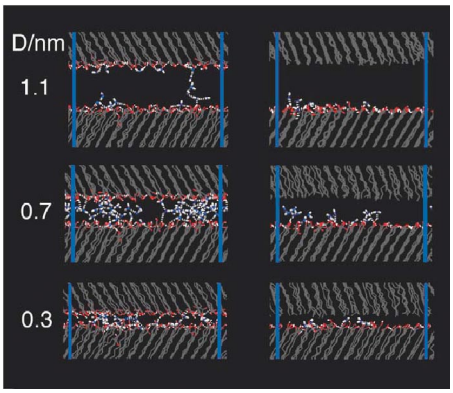

FIG. 2 (color). Snapshots of the gap regions for COOH/COOH (left column) and CH_3/COOH (right column) systems taken from the MC simulations during approach ($D = 1.1$, 0.7, and 0.3 nm). The oxygen atoms in water or COOH groups are blue or red, respectively. The dashed white lines represent hydrogen bonds. The thick blue lines depict the boundaries of the periodically replicated system.

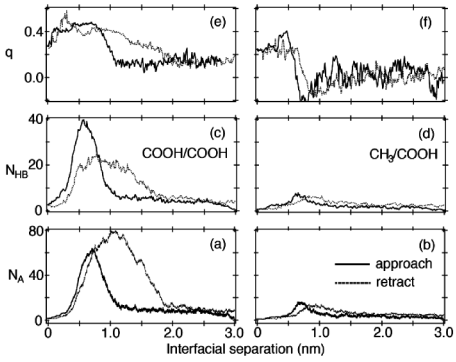

FIG. 3. The number of water molecules within the simulation cell (N_A, bottom row), the number of hydrogen bonds to each acid surface (N_{HB}, middle row), and the tetrahedral order parameter of water molecules (q, top row) as a function of interfacial separation for the COOH/COOH (left column) and CH_3/COOH (right column) systems. The solid and dashed curves depict the approach and retract data, respectively.

This difference is a consequence of the simulation setup using an ideal Au substrate and two-dimensional periodicity; i.e., upon retraction a vapor bubble needs to nucleate within the water film.

Further information on the structure of the water meniscus is obtained from analysis of the number of hydrogen bonds between water molecules and each acid surface (N_{HB}) and of the orientational order parameter (q). The former quantity is determined using the hydrogen bond criterion suggested by Wernet *et al.* [27] and normalized by the number of acid surfaces. The orientational order parameter introduced by Errington and Debenedetti [28] measures the degree of tetrahedral ordering in bulk water and falls in the range of -3 to 1; because the q parameter was developed for three-dimensional systems, its qualitative use here for a two-dimensional system should be restricted to relative comparisons (e.g., at different interfacial separations). As shown in Figs. 3(c) and 3(d), at large separations, N_{HB} is the same for the COOH/COOH and the COOH/CH_3 systems. At short separations there is a cooperative effect for the COOH/COOH system and N_{HB} exceeds that for the COOH/CH_3 system by approximately a factor of 2. This cooperative effect is also seen in q [Figs. 3(e) and 3(f)]. In the COOH/COOH system, the rise in N_{HB} or N_A is accompanied by an increase in q, while for the COOH/CH_3 system, q first decreases in the region of capillary condensation and only increases (to a lower peak value than that in COOH/COOH) when N_{HB} or N_A start to decrease. The interfacial distances at which q rises and N_{HB} peaks for the COOH/COOH system are in excellent agreement with the experimentally observed distance range where friction peaks. Thus, the cooperative effect of hydrogen bonding to the two COOH surfaces is likely responsible for the high viscosity.

Sandia is a multiprogram laboratory operated by Sandia Corporation, a Lockheed Martin Company, for the DOE's National Nuclear Security Administration under Contract No. DE-AC04-94AL85000. Partial support from NSF (CHE-0213387) and Minnesota Supercomputing Institute is also acknowledged. We thank P. Feibelman, T. Lodge, and H. Petek for a critical reading of this manuscript.

[1] J. Israelachvilli and H. Wennerström, Nature (London) **379**, 219 (1996).
[2] S. Karaborni, B. Smit, W. Heidug, J. Urai, and E. van Oort, Science **271**, 1102 (1996).
[3] J. Jang, G. C. Schatz, and M. A. Ratner, Phys. Rev. Lett. **90**, 156104 (2003).
[4] R. D. Piner, J. Zhu, F. Xu, S. Hong, and C. A. Mirkin, Science **283**, 661 (1999).
[5] Q. Du, E. Freysz, and Y. R. Shen, Phys. Rev. Lett. **72**, 238 (1994).
[6] V. Ostroverkhov, G. A. Waychunas, and Y. R. Shen, Phys. Rev. Lett. **94**, 046102 (2005).
[7] D. B. Asay and S. H. Kim, J. Phys. Chem. B **109**, 16 760 (2005).
[8] J. Hu, D. F. Xiao, D. F. Ogletree, and M. Salmeron, Science **268**, 267 (1995).
[9] M. F. Toney *et al.*, Nature (London) **368**, 444 (1994).
[10] J. Israelachvili, *Intermolecular & Surface Forces* (Academic Press, New York, 1992).
[11] H.-W. Hu, G. A. Carson, and S. Granick, Phys. Rev. Lett. **66**, 2758 (1991).
[12] Y. Zhu and S. Granick, Phys. Rev. Lett. **87**, 096104 (2001).
[13] M. Antognozzi, A. D. L. Humphris, and M. J. Miles, Appl. Phys. Lett. **78**, 300 (2001).
[14] U. Raviv, P. Laurat, and J. Klein, Nature (London) **413**, 51 (2001).
[15] J. N. Israelachvili, J. Colloid Interface Sci. **110**, 263 (1986).
[16] M. Binggeli and C. M. Mate, Appl. Phys. Lett. **65**, 415 (1994).
[17] J. E. Houston and H. I. Kim, Acc. Chem. Res. **35**, 547 (2002).
[18] R. Arnold, W. Azzam, A. Terfort, and C. Wöll, Langmuir **18**, 3980 (2002); T. M. Willey *et al.*, Langmuir **20**, 2746 (2004).
[19] R. C. Major and X. Y. Zhu, J. Am. Chem. Soc. **125**, 8454 (2003).
[20] P. J. Feibelman, Langmuir **22**, 2136 (2006).
[21] B. Pittenger *et al.*, Phys. Rev. B **63**, 134102 (2001).
[22] H. I. Kim, J. G. Kushmerick, J. E. Houston, and B. C. Bunker, Langmuir **19**, 9271 (2003).
[23] J. I. Siepmann and I. R. McDonald, Phys. Rev. Lett. **70**, 453 (1993).
[24] J. I. Siepmann and I. R. McDonald, Langmuir **9**, 2351 (1993).
[25] M. G. Martin and J. I. Siepmann, J. Phys. Chem. B **102**, 2569 (1998).
[26] W. L. Jorgensen *et al.*, J. Chem. Phys. **79**, 926 (1983).
[27] Ph. Wernet *et al.*, Science **304**, 995 (2004).
[28] J. R. Errington and P. G. Debenedetti, Nature (London) **409**, 318 (2001).